J. Fluid Mech. (2016), *vol.* 798, *pp.* 232–255.
doi:10.1017/jfm.2016.293

Waves from an oscillating point source with a free surface in the presence of a shear current

Simen Å. Ellingsen[1,†] **and Peder A. Tyvand**[2]

[1]Department of Energy and Process Engineering, Norwegian University of Science and Technology, N-7491 Trondheim, Norway

[2]Department of Mathematical Sciences and Technology, Norwegian University of Life Sciences, N-1432 Ås, Norway

(Received 7 July 2015; revised 9 March 2016; accepted 20 April 2016; first published online 31 May 2016)

We investigate analytically the linearised water wave radiation problem for an oscillating submerged point source in an inviscid shear flow with a free surface. A constant depth is taken into account and the shear flow increases linearly with depth. The surface velocity relative to the source is taken to be zero, so that Doppler effects are absent. We solve the linearised Euler equations to calculate the resulting wave field as well as its far-field asymptotics. For values of the Froude number $F^2 = \omega^2 D/g$ (where ω is the oscillation frequency, D is the submergence depth and g is the gravitational acceleration) below a resonant value F^2_{res}, the wave field splits cleanly into separate contributions from regular dispersive propagating waves and non-dispersive 'critical waves' resulting from a critical layer-like street of flow structures directly downstream of the source. In the subresonant regime, the regular waves behave like sheared ring waves, while the critical layer wave forms a street with a constant width of order $D\sqrt{S/\omega}$ (where S is the shear flow vorticity) and is convected downstream at the fluid velocity at the depth of the source. When the Froude number approaches its resonant value, the downstream critical and regular waves resonate, producing a train of waves of linearly increasing amplitude contained within a downstream wedge.

Key words: critical layers, shear waves, waves/free-surface flows

1. Introduction

The submerged oscillatory point source is pivotal for three-dimensional (3D) water waves with a localised cause. Kochin (1939, 1940) gave the first mathematical solutions where the source satisfies the linearised free-surface conditions and radiation conditions at infinity. Wehausen & Laitone (1960) summarised the classical solutions for submerged oscillatory sources. They are useful as Green functions for solving diffraction and radiation problems in marine hydrodynamics (Newman 1977; Faltinsen 1990). The description of submerged bodies in inviscid flow using flow singularities rather than a full boundary value solution is highly economical, and has been hugely successful for irrotational flow. No corresponding Green function theory exists when

† Email address for correspondence: simen.a.ellingsen@ntnu.no

a shear current is present, however, and as a first step in this direction we consider the properties of the basic building block for such a theory: the submerged oscillating point source.

In the preceding paper (Ellingsen & Tyvand 2016, abbreviated E&T hereafter), we showed how the standard theory of the oscillating line source in two dimensions with free surface and uniform shear based on potential theory is inadequate. Potential theory has traditionally been applied to this system on the grounds that when vorticity is constant the wave motion will be irrotational due to conservation of circulation by Kelvin's circulation theorem. The 2D radiation problem was solved under this assumption by Tyvand & Lepperød (2014, 2015) with both zero and non-zero surface velocity relative to the oscillating source respectively. However, we recently discovered that due to the violation of Laplace's equation at the source position itself, it is necessary to treat the problem with the full Euler equations (see E&T). The resulting wave pattern obtains a correction from the formation of a critical layer-like train of downstream vortices at the source depth, which can completely dominate the wave picture in certain parameter regimes, and which drastically alters the wave picture downstream of the source (as seen from a system where source and undisturbed surface are at rest). The existence of critical layer-type solutions in two dimensions and uniform shear had previously been pointed out in the mathematical literature (Ehrnström & Villari 2008; Wahlén 2009), confirming an age old conjecture by Lord Kelvin (Thomson 1880). The problem is a classic one and has attracted considerable recent attention; see Constantin & Varvaruca (2011) for a review.

In the present paper, we will extend the work in two dimensions from E&T to three dimensions, still using the simplifying assumption that the source is at rest relative to the surface of the fluid. While this is a restriction that we will want to lift in the future, this assumption is a significant simplification because complicating Doppler effects are avoided, allowing us to study several novel features unobscured by additional complexity.

In three dimensions and in the presence of shear current, potential theory is certainly not an option (e.g. Ellingsen & Brevik 2014). Possibly for this reason the literature on 3D water waves with vorticity is small; a ring wave theory by Johnson (1990) and some works in an oceanographic context, e.g. Shrira (1993) and Mellor (2003), are notable examples. Progress was made recently, when it was realised by one of us that a simple solution exists to the linearised Euler equation in three dimensions in the presence of uniform shear, and the solution was used to solve the linear ship wave problem (Ellingsen 2014*b*), as well as the corresponding Euler–Cauchy problem of an initial disturbance (Ellingsen 2014*a*). Both efforts have been generalised and expanded by Li & Ellingsen (2015, 2016). The present theory follows essentially the same procedure with the only significant difference being the presence of the source making the continuity equation inhomogeneous.

In a famous review, Peregrine (1976) names several situations where the depth dependence of a current will affect surface waves. Noting that shear is typically present either near the surface (for example due to wind shear, as considered by, e.g., Shemdin (1972) and Jones & Toba (2001)) or in a boundary layer near the bottom (e.g. Soulsby *et al.* 1993), and that a wave can 'see' approximately half its wavelength into the deep, the presence of vorticity will affect waves whose wavelength is either sufficiently short to be affected strongly by the surface layer or so long as to be affected by the entire water column. Situations where shear may be significant also include tidal currents (e.g. Dyer 1971). The Green functions summarised in the famous review of Wehausen & Laitone (1960) are all for irrotational flow. To the

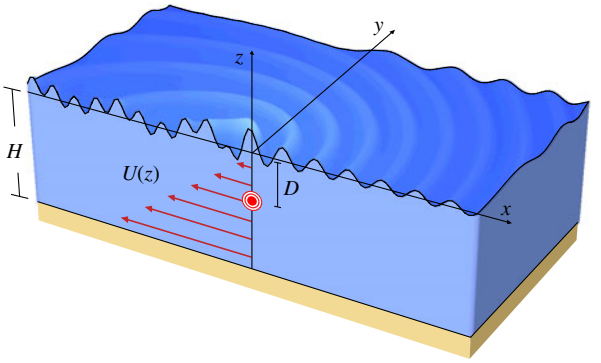

FIGURE 1. (Colour online) The geometry considered: an oscillating point source sits at depth D in a uniform shear current so that the source is at rest relative to the undisturbed water surface.

best of our knowledge it still holds true today that the literature on fluid mechanical Green functions is restricted to potential flow solutions. Hence, no valid Green function theory exists for floating bodies in shear currents, and the current effort takes perhaps the first step in this direction.

In comparing the 2D result of E&T with the 3D treatment herein, it should be noted that while the background flow in our 3D geometry is presumed to possess a constant vorticity, this is not the case for the flow as a whole. It was shown by Constantin (2011) and others that an assumption of constant non-zero vorticity implies that the flow is strictly 2D. This apparent paradox was recently addressed by Ellingsen (2016), demonstrating that a plane wave propagating at an oblique angle with a subsurface shear flow of uniform vorticity will shift the vortex lines of the basic flow and be, in an Eulerian sense, rotational, and the total fluid motion has non-constant vorticity. Thus, there is no conflict between Constantin's theorem and the present work.

2. Mathematical model

We consider an inviscid and incompressible fluid in a steady shear flow, where the shear flow is aligned with a horizontal x axis. The fluid has constant depth and a free surface subject to constant atmospheric pressure. Cartesian coordinates x, y, z are introduced, where the z axis is directed upwards in the gravity field and the x, y plane represents the undisturbed free surface. The gravitational acceleration is g, and ρ denotes the constant fluid density. We neglect surface tension throughout. The velocity perturbation vector is denoted by $\boldsymbol{v} = (\hat{u}, \hat{v}, \hat{w})$ and the full pressure is $P = -\rho g z + \hat{p}$, where $\hat{p}$ is the perturbation. The surface elevation is denoted by $\zeta(x, y, t)$ and the overall problem is sketched in figure 1. There is a wave motion driven by a fixed oscillating point source located at the point $(0, 0, -D)$. The water wave problem will be linearised with respect to the surface elevation and the velocity and pressure perturbations.

We assume constant fluid depth H. There is a basic horizontal shear flow $U(z)$ in the x direction,

$$U(z) = Sz, \quad z < \zeta. \tag{2.1}$$

The basic flow thus contains a uniform vorticity S in the y direction, whose influence on the surface motion is our principal concern.

Euler's equation of motion can be written as

$$\boldsymbol{a} = -\frac{1}{\rho}\nabla P - g\boldsymbol{e}_z, \tag{2.2}$$

where $\boldsymbol{a}$ is the acceleration vector and $\boldsymbol{e}_i$, $i \in \{x, y, z\}$, are the Cartesian unit vectors.

The linearised kinematic free-surface condition is

$$\hat{w}|_{z=0} = \zeta_t, \tag{2.3}$$

with subscripts denoting partial derivatives.

In the absence of both surface tension and viscosity, the dynamic boundary condition is simply that the pressure be constant (chosen equal to zero) on the free surface. This may be written by means of the tangential component of the Euler equation,

$$[\boldsymbol{a} - (\boldsymbol{a}\cdot\boldsymbol{n})\boldsymbol{n} + g\boldsymbol{e}_z - g(\boldsymbol{e}_z\cdot\boldsymbol{n})\boldsymbol{n}]|_{z=\zeta} = 0, \tag{2.4}$$

because $\nabla P - \boldsymbol{n}(\boldsymbol{n}\cdot\nabla P) = 0$ there. Here, the surface normal vector is denoted by $\boldsymbol{n}$. According to linear theory, the surface normal is given by $\boldsymbol{n} = \boldsymbol{k} - \nabla\zeta$. We linearise this dynamic free-surface condition and decompose it in the x and y directions, giving

$$(\hat{u}_t + S\hat{w})|_{z=0} = -g\zeta_x, \tag{2.5a}$$

$$\hat{v}_t|_{z=0} = -g\zeta_y. \tag{2.5b}$$

By combining these two dynamic conditions we obtain

$$(\hat{u}_{xt} + \hat{v}_{yt} + S\hat{w}_x)|_{z=0} = -g(\zeta_{xx} + \zeta_{yy}), \tag{2.6}$$

and use the incompressibility of the flow to eliminate the horizontal velocities to obtain

$$(\hat{w}_{zt} - S\hat{w}_x)|_{z=0} = g(\zeta_{xx} + \zeta_{yy}). \tag{2.7}$$

The dynamic free-surface condition is thus expressed in terms of the vertical velocity and the elevation.

The last boundary condition is the bottom condition,

$$\hat{w} = 0, \quad z = -H. \tag{2.8a,b}$$

We will work with finite H, giving special attention to the limit $H \to \infty$.

We assume time-periodic flow with given angular frequency ω. This flow is driven by a point source of harmonically pulsating strength $Q(t) = Q_0\cos(\omega t)$. The source strength $Q(t)$ is the instantaneous volume flux emitted from the singular source, which is located at the constant depth $z = -D$. We will go to complex notation for the time dependence henceforth. The mass balance is given by the continuity equation

$$\nabla\cdot\boldsymbol{v} = Q_0\delta(x)\delta(y)\delta(z+D)\mathrm{e}^{-\mathrm{i}\omega t}. \tag{2.9}$$

We shall seek solutions so that the temporal behaviour of all perturbations is through a factor $\exp(-\mathrm{i}\omega t)$, i.e. the periodic steady-state solution.

The variables are Fourier transformed as follows:

$$(\hat{u}, \hat{v}, \hat{w}, \hat{p}) = Q_0\int \frac{\mathrm{d}^2k}{(2\pi)^2}(u(z), v(z), w(z), p(z))\mathrm{e}^{\mathrm{i}\boldsymbol{k}\cdot\boldsymbol{r}_\perp - \mathrm{i}\omega t}, \tag{2.10}$$

where the real part has physical significance. We have introduced the horizontal position vector $\boldsymbol{r}_\perp = (x, y) = (r\cos\phi, r\sin\phi)$ and the wavevector $\boldsymbol{k} = (k_x, k_y) = (k\cos\theta, k\sin\theta)$, in Cartesian and polar phase space coordinates respectively. It should be noted that $k = |\boldsymbol{k}|$, which, unlike components k_x, k_y, is $\geqslant 0$, an important point to bear in mind when comparing with theory for the corresponding 2D flow in E&T, where k is used in the sense k_x. We let θ and ϕ take values between $-\pi$ and π.

We shall use the terms upstream and downstream in the sense that they were used by E&T, by considering the source and undisturbed surface to be stationary. Thus, we refer to directions $|\theta| < \pi/2$ as propagating upstream (ahead of the source), and $|\theta| > \pi/2$ are denoted as downstream propagation directions. This would be opposite were we to consider the surface to be in motion, as was the case, e.g., in Ellingsen & Brevik (2014).

The transformed components of the Euler equation are given by

$$-\mathrm{i}(\omega - k_x U)u + Sw = -\mathrm{i}k_x p/\rho, \tag{2.11a}$$

$$-\mathrm{i}(\omega - k_x U)v = -\mathrm{i}k_y p/\rho, \tag{2.11b}$$

$$-\mathrm{i}(\omega - k_x U)w = -p'/\rho, \tag{2.11c}$$

where a prime denotes a derivative with respect to z. The transformed continuity equation is

$$\mathrm{i}k_x u + \mathrm{i}k_y v + w' = \delta(z + D). \tag{2.12}$$

In exactly the same way, the surface elevation is Fourier transformed according to

$$\zeta(x, y, t) = Q_0 \int \frac{\mathrm{d}^2 k}{(2\pi)^2} B(\boldsymbol{k}) \mathrm{e}^{\mathrm{i}\boldsymbol{k}\cdot\boldsymbol{r}_\perp - \mathrm{i}\omega t}. \tag{2.13}$$

2.1. *Vorticity dynamics*

Before continuing, let us take a moment to consider the vorticity equation for the system at hand, which to linear order in perturbations reads

$$\frac{\mathrm{D}\boldsymbol{\Omega}}{\mathrm{D}t} = S\frac{\partial \boldsymbol{v}}{\partial y} - S\boldsymbol{e}_y(\boldsymbol{\nabla}\cdot\boldsymbol{v}) = S\frac{\partial \boldsymbol{v}}{\partial y} - SQ_0\delta(x)\delta(y)\delta(z + D)\mathrm{e}^{-\mathrm{i}\omega t}\boldsymbol{e}_y, \tag{2.14}$$

where $\boldsymbol{\Omega} = \boldsymbol{\nabla}\times\boldsymbol{v}$ is the perturbation vorticity, the background flow has vorticity $S\boldsymbol{e}_y$ and we have inserted (2.9). The two terms on the right-hand side correspond to two different mechanisms whereby the vorticity of a fluid particle might change as it travels with the flow.

The term proportional to $\delta(x)\delta(y)\delta(z + D)$ was discussed at length in E&T. A fluid particle passing through the source point is given additional vorticity because its volume is momentarily changed while its circulation remains the same. The additional vorticity due to the inhomogeneity in the vorticity equation (the term proportional to $\delta(z = D)$) is expected to be proportional to $-SQ_0\exp(-\mathrm{i}\omega t)/U(-D)$, because the time such a small volume of fluid spends with the source inside it is proportional to $1/U(-D)$.

The term $S\partial\boldsymbol{v}/\partial y$ comes from the fact that a wave propagating at an oblique angle over a shear current will gently shift and twist the vortex lines as it passes, as discussed by Ellingsen (2016). The effect may be understood in terms of the plane wave components of the wave picture (2.13) by noting that $\partial/\partial y \to \mathrm{i}k_y$ in Fourier space. Thus, it is the combination of the subsurface shear S and an oblique propagation direction relative to the current, $k_y \neq 0$, that causes the vorticity of fluid particles to change as they are convected.

3. Formal solution of the radiation problem

From the transformed governing equations, we can eliminate u, v and p to obtain an equation for the vertical velocity alone,

$$w'' - k^2 w = \delta'(z+D) - \frac{k_x S}{\omega - k_x U}\delta(z+D). \tag{3.1}$$

Since $\delta(z+D)$ is non-zero only at $z=-D$, the fraction $k_x S/(\omega - k_x U)$ effectively becomes $k_x S/(\omega + k_x SD)$ in the last term. The homogeneous solution of this equation that satisfies the bottom condition is written in the form

$$w_h(z) = A(\boldsymbol{k}) \sinh k(z+H), \tag{3.2}$$

where $A(\boldsymbol{k})$ is an undetermined velocity amplitude. In addition, there are two particular solutions to (3.1) due to the two forcing terms on the right-hand side,

$$w_{p1}(z) = \cosh k(z+D)\Theta(z+D), \tag{3.3}$$

$$w_{p2}(z) = -\frac{k_x S}{k(\omega + k_x SD)} \sinh k(z+D)\Theta(z+D), \tag{3.4}$$

where the Heaviside unit step function $\Theta(z)$ has been introduced. The solution is strikingly similar to that obtained in the 2D case of E&T.

From transforming the kinematic free-surface condition (2.3) we find the relationship

$$A \sinh kH = -\cosh kD + \frac{k_x S \sinh kD}{k(\omega + k_x SD)} - \mathrm{i}\omega B. \tag{3.5}$$

Similarly, the dynamic free-surface condition (2.7) gives

$$\begin{aligned}(\omega k \coth kH + k_x S)A \sinh kH + \omega k \sinh(kD) + k_x S \cosh kD \\ - \frac{\omega k_x S \cosh kD + (k_x^2 S^2/k)\sinh kD}{\omega + k_x SD} = -\mathrm{i}gk^2 B.\end{aligned} \tag{3.6}$$

From the two last equations we eliminate A, since we are most interested in the surface elevation. It is expressed by $B(\boldsymbol{k})$ so that

$$\frac{\mathrm{i}g}{\omega}\left(k - \frac{\omega}{g}S\cos\theta - \frac{\omega^2}{g}\coth kH\right)B(\boldsymbol{k}) = \frac{\cosh k(H-D)}{\sinh kH} + \frac{S\cos\theta \sinh k(H-D)}{(\omega + kSD\cos\theta)\sinh kH}. \tag{3.7}$$

4. Dispersion relation and the radiation condition

In (3.7), $B(\boldsymbol{k})$ is multiplied by a factor that will be zero when $\boldsymbol{k}$ has a value corresponding to the dispersion relation for a given ω,

$$k - \frac{\omega}{g}S\cos\theta - \frac{\omega^2}{g}\coth kH = 0. \tag{4.1}$$

This is identical to the dispersion relation derived and discussed at length by Ellingsen (2014*a*), except that here it is ω, not $\boldsymbol{k}$, that is taken to be the known quantity. The dispersion relation was derived by Tyvand & Lepperød (2014) for the cases $\theta = 0$ and $\theta = \pi$ corresponding to 2D flow. See also the more detailed discussion of the 2D dispersion relation by Ellingsen & Brevik (2014). This selected value of the wavevector gives a pole in the solution integral (2.13).

4.1. *Dispersion relation in deep water*

Let us analyse the dispersion relation (4.1), which we treat as a function of $\boldsymbol{k}$ with ω a fixed parameter. The following discussion generalises that found in appendix A of E&T. Wishing to consider the simpler case of infinitely deep water, $H \to \infty$, the naive procedure is to let $\coth kH \to 1$ in (4.1), whereby the dispersion relation becomes simple and explicit with respect to k:

$$k(\theta) = \frac{\omega}{g}(\omega + S\cos\theta). \tag{4.2}$$

We immediately see a potential problem with relation (4.2), because when $S > \omega$ it seems to permit negative values of $k(\theta)$, which is nonsensical and must be remedied by manually excluding the corresponding values of θ from the final integral.

The reason for this conundrum may be found in the fact that the mathematical limit taken in dispersion relation (4.1) is $kH \to \infty$, which is the same as the deep-water limit $H \to \infty$ only if k does not simultaneously tend to zero. A numerical solution $k(\theta)$ of dispersion relation (4.1) when H grows large shows that in the 'forbidden sectors' where (4.2) is negative, the solution $k(\theta)$ tends quickly to zero so that $k(\theta)H$ remains finite near $\theta = \pm\pi$. In other words, the forbidden sector is a phenomenon that only occurs at infinite depth, while for any finite H a positive solution $k(\theta)$ exists in all directions.

We can study this a little more closely by writing (4.1) in the form

$$\coth\chi - \eta\chi = -(S/\omega)\cos\theta, \tag{4.3}$$

where $\chi = k(\theta)H$ and $\eta = g/H\omega^2$. When the water is deep, $\eta \ll 1$. The sectors in which (4.2) predicts negative K values are clearly where $\cos\theta < 0$, near $\theta = \pm\pi$. Assuming therefore that the right-hand side of (4.3) is positive and > 1, there clearly exists a solution for moderate values of χ where the term containing η can be neglected, approximated by

$$k(\theta)H = \chi \overset{H\to\infty}{\approx} \operatorname{arcoth}(-S\cos\theta/\omega) = \frac{1}{2}\ln\frac{\omega - S\cos\theta}{-\omega - S\cos\theta} \tag{4.4}$$

provided that $-\omega - S\cos\theta > 0$. Thus, when $S > \omega$ the product $k(\theta)H$ never grows large near $\theta = \pm\pi$ as $H \to \infty$, and the naive taking of the deep-water limit leads to unphysical solutions.

Numerical solutions to the dispersion relation (4.1) for the case $S = 2\omega$ are shown in figure 2 for different values of the (suitably non-dimensionalised) depth H, where the relation (4.2) is also shown. This figure also shows the behaviour of $k(\theta)H$ near $\theta \to \pi$ when H grows large. It is clear from the numerical solutions that the correct limiting dispersion relation is in fact not (4.2), but instead

$$k_0(\theta) \overset{H\to\infty}{=} \frac{\omega}{g}(\omega + S\cos\theta)\Theta(\omega + S\cos\theta), \tag{4.5}$$

with Θ again the Heaviside function. What this implies is that in propagation directions where $\omega + S\cos\theta < 0$, the permissible plane wave solution approaches infinite wavelength. In a similar manner to that of the appendix of E&T, one can show that there is no energy transport in this 'forbidden sector' in the limit $H \to \infty$,

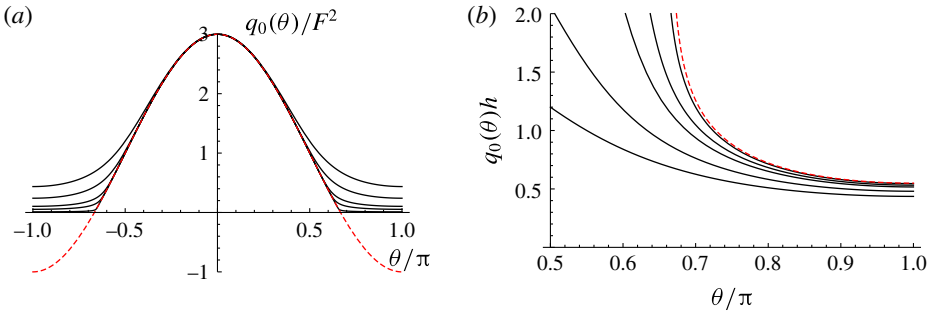

FIGURE 2. (Colour online) (*a*) Plots of wavenumbers $k_0(\theta)$ that solve (4.1), non-dimensionalised as in table 1, for different values of $F^2h = 1, 2, 5, 10, 50$ (solid lines, top to bottom) with $S/\omega = 2$. The naive expression (4.2) is plotted as a dashed line. (*b*) Plots of $q_0(\theta)h$ for the same solutions, plotted near $\theta = \pi$, again for $F^2h = 1, 2, 5, 10, 50$ (solid lines, bottom to top). The asymptotic solution (4.4) is shown as a dashed line.

and hence this sector is to be simply excluded from the integral over $\boldsymbol{k}$ in the deep-water limit by means of a cutoff: values of θ must satisfy

$$|\theta| < \arccos[\max(-\omega/S, -1)] \equiv \theta_0. \tag{4.6}$$

For any $H < \infty$, the integral is not cut off explicitly. That said, when $S/\omega > 1$ and $h \gg g/\omega^2$ (deep waters), the sector that at infinite depth would be forbidden is characterised by regular waves of very long wavelength and correspondingly small amplitude.

4.2. *Radiation condition*

Before we proceed, let us non-dimensionalise all quantities with respect to length D and time $1/\omega$, in particular

$$\boldsymbol{q} = D\boldsymbol{k}, \quad \tilde{\boldsymbol{r}} = \boldsymbol{r}_\perp/D, \quad T = \omega t, \tag{4.7a–c}$$

and we obtain the dimensionless parameters

$$\sigma = S/\omega, \tag{4.8}$$

$$F = \omega\sqrt{D/g}. \tag{4.9}$$

An exception from this non-dimensional scaling is made for the perturbed quantities, which are scaled instead with respect to the length scale

$$\zeta_0 = \frac{Q_0\omega}{gD}. \tag{4.10}$$

Here, σ is the dimensionless shear (or vorticity) and F^2 is a Froude number based on length D and velocity ωD. The various non-dimensional quantities are listed in table 1. The expression for the surface elevation now becomes

$$\tilde{\zeta} = \frac{\mathrm{e}^{-\mathrm{i}T}}{4\pi^2\mathrm{i}} \int_{-\pi}^{\pi} \mathrm{d}\theta \int_0^\infty \mathrm{d}q\, q \frac{\mathrm{e}^{\mathrm{i}q\tilde{r}\cos(\theta-\phi)}}{\Gamma(\boldsymbol{q})\sinh qh} \left[\cosh q(h-1) + \frac{\sinh q(h-1)}{q - q_c}\right], \tag{4.11a}$$

$$\Gamma(\boldsymbol{q}) = q - F^2(\coth qh + \sigma\cos\theta), \tag{4.11b}$$

Dimensional quantity	Non-dimensional quantity	Name
S	$\sigma = S/\omega$	Shear parameter
H	$h = H/D$	Relative depth
ζ	$\tilde{\zeta} = \zeta/\zeta_0$	Non-dimensional elevation
x, y, z	$(\tilde{x}, \tilde{y}, \tilde{z}) = (x, y, z)/D$	Non-dimensional position
t	$T = t\omega$	Phase
$\boldsymbol{k}$	$\boldsymbol{q} = D\boldsymbol{k}$	Wavevector

TABLE 1. Table of non-dimensional quantities.

where $\tilde{\zeta} = \zeta/\zeta_0$, $h = H/D$, $\tilde{r}^2 = \tilde{x}^2 + \tilde{y}^2$. We also define the critical dimensionless wavenumber

$$q_c = -\frac{1}{\sigma \cos\theta}. \tag{4.12}$$

Insertion of the solution for $B(\boldsymbol{k})$ in (3.7) into (2.13) now produces an integral that is not well defined because it contains poles on the integration axis. The problem is a standard one encountered in all periodic or stationary wave systems, and must be resolved by means of a radiation condition ensuring that only outgoing waves are included while formal solutions to the strictly periodic problem that correspond to waves originating at infinity must be excluded. As in E&T we employ the radiation condition in the manner of, e.g., Lighthill (1978, § 4.9) by presuming that the point source has been switched on slowly and gradually since $t = -\infty$, by replacing

$$Q_0 \to Q_0 \mathrm{e}^{\epsilon\omega t}, \tag{4.13}$$

where ϵ will be taken to zero in the end through positive values (this definition is permissible for $\omega > 0$ and makes ϵ dimensionless, which is convenient). This amounts to a replacement rule everywhere,

$$\omega \to \omega(1 + \mathrm{i}\epsilon). \tag{4.14}$$

As ϵ is taken towards zero, its sole significance is that it moves the poles in the integrand slightly off the real q axis. In exact analogy to the 2D case considered in E&T, there are two types of poles in the integrand, corresponding to two types of waves. First, there are the standard dispersive waves at values $q_0(\theta)$ that satisfy $\Gamma(\boldsymbol{q}) = 0$, i.e.

$$q_0 = F^2[\coth(q_0 h) + \sigma \cos\theta], \tag{4.15}$$

which defines $q_0(\theta)$ implicitly. Second, there is a pole at $q = q_c$ because of the presence of a critical layer-like downstream flow, as discussed at length in E&T. It was shown in E&T how the critical layer in two dimensions is a sequence of vortices which is advected downstream with the flow at the velocity $U_c = -SD$ which the fluid has at depth D. The nature of the critical layer solution in the present 3D geometry will be analysed further below.

The replacement rule (4.14) gives a revised expression for $\tilde{\zeta}$ which is now uniquely defined:

$$\tilde{\zeta} = \frac{\mathrm{e}^{-\mathrm{i}T}}{4\pi^2 \mathrm{i}} \int_{-\pi}^{\pi} \mathrm{d}\theta \lim_{\epsilon \to 0^+} G(\theta), \tag{4.16}$$

$$G(\theta) = \int_0^\infty \mathrm{d}q\, q \frac{\mathrm{e}^{\mathrm{i}q\tilde{r}\cos(\theta-\phi)}}{[\Gamma(\boldsymbol{q}) - \mathrm{i}\epsilon\Phi(\boldsymbol{q})]\sinh qh} \left[\cosh q(h-1) + \frac{\sinh q(h-1)}{q - q_c(1+\mathrm{i}\epsilon)}\right], \quad (4.17)$$

$$\Phi(\boldsymbol{q}) = F^2(2\coth qh + \sigma\cos\theta). \quad (4.18)$$

This expression may now be used directly for numerical purposes by choosing a small but non-zero value of ϵ. In the following, we will also extract the far-field part of the solution in a manner similar to that of E&T.

5. Far-field solution

As discussed extensively in the literature (cf., e.g., Wehausen & Laitone 1960; Lighthill 1978), it is the poles of the integral over $\boldsymbol{q}$, i.e. the poles of (4.11), that contribute to the far zone. This is true also in the present case, as we argue below. Regard the integral as written in (4.16), so that the integral of the wavenumber (or wavevector modulus) q is taken first, then the integral over propagation directions θ second. The physical significance of the pole near $q = q_0(\theta)$ is well known: $q = q_0$ is simply the dispersion relation that must be satisfied in order for waves to propagate towards infinity.

The second pole, at $q = q_c(\theta)$, is physically interesting and was discussed for the 2D case in E&T. The pole at $q = q_c$ occurs for the wavenumber at which waves at depth $z = -D$ propagating in direction θ have a phase velocity that, when measured along the direction of the current, $-\boldsymbol{e}_x$, is equal to the velocity of the fluid flow, $U(-D) = -SD$. This is the condition for the formation of a critical layer, a phenomenon that has been studied extensively in two dimensions. We showed (E&T) that even for a linear shear current of uniform vorticity in two dimensions, a critical layer-like flow is created by a submerged oscillating source. The existence of critical layer-type solutions for the constant vorticity flow in two dimensions was previously reported in the mathematical literature (Ehrnström & Villari 2008; Wahlén 2009), and takes the form of a train of vortical fluid structures similar to Kelvin's cat's eye vortices, centred at the source depth and advected downstream with the shear flow. In three dimensions, the same phenomenon occurs, and we will show that the surface deformation associated with the critical layer typically takes the form of a narrow train of waves which retains constant shape as it is convected downstream.

It should be noted that while we refer to the vortical flow drifting downstream of the source as a critical layer flow due to its obvious similarities with critical layers as they occur in the literature on waves on shear flows (e.g. Booker & Bretherton 1967), there is an important difference regarding how the critical wave interacts with the propagating surface waves. In the present case, the critical layer is not caused by a propagating wave impinging on a critical level, but is created by the source itself, and does not interact with the propagating regular waves except near a particular resonance frequency, which we discuss in detail in the following.

In order to evaluate the far field, we close the integration contour in the complex q plane as shown in figure 3. In order for the contribution from the poles to be identifiable as the far-field contribution, it is necessary to close the contour above or below according to the sign of the exponent factor $\cos(\theta - \phi)$ to ensure that the integrand along each leg of the contour is a decreasing function of $\tilde{r}$ as $\tilde{r} \to \infty$. We choose to close the contour by means of a circular arc at infinity and a straight path making an angle with the real axis which we may choose arbitrarily so long as it is strictly greater than zero (to ensure that the abovementioned poles are enclosed when they should be) and small enough to exclude a series of poles a little to the side of

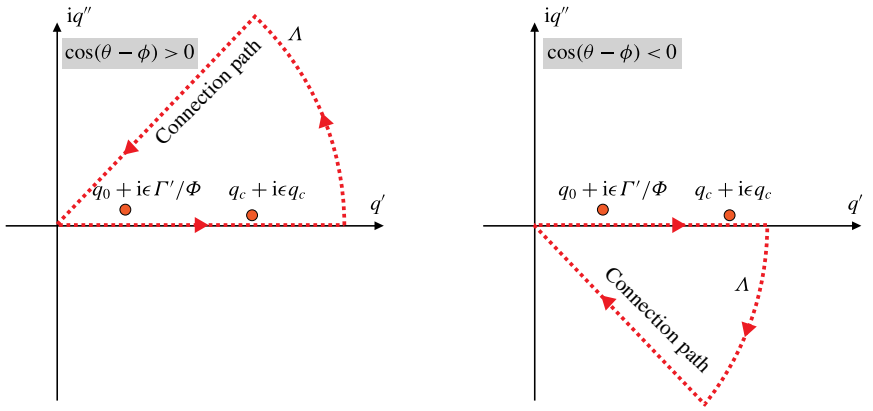

FIGURE 3. (Colour online) Contours in the complex q plane used for extracting the far-field solution. Here q' and q'' denote the real and imaginary parts of q, respectively.

the imaginary axis where $\Gamma(\boldsymbol{q})$ has zeros. These poles contribute to the near field only, and lie a little to the right or the left of the imaginary axis depending on $\cos\theta$ as well as h, σ and F^2. For numerical purposes, we choose a path making an angle $\gamma = \pm 0.4\pi$ with the real axis, which causes no problems with the parameters we consider (it is numerically beneficial to be as close as possible to the path of steepest descent, which in the deep-water case is at $\tan\gamma = \tilde{r}\cos(\theta - \phi)$, yet this path will lie perilously close to the imaginary axis for large $\tilde{r}$).

Consider now the two poles in the integrand of (4.11). Upon replacing $\omega \to \omega(1 + \mathrm{i}\epsilon)$ the poles have been shifted to the positions

$$q_c \to q_c(1 + \mathrm{i}\epsilon), \tag{5.1}$$

$$q_0 \to q_0 + \mathrm{i}\epsilon\Phi(q_0)/\Gamma'(q_0). \tag{5.2}$$

Since the contribution from the pole to the integral $G(\theta)$ contributes the far field, it is clear that a far-field contribution from either regular or critical waves exists only for values of σ, F^2 and θ for which the pole lies inside the contour. A similar analysis is performed for the case of ship waves by Li & Ellingsen (2016).

Assume now that $q_0 \neq q_c$, so that the two poles are well separated and may be treated independently (according to the terminology we will introduce in § 5.1, a situation where this is true for all θ is called subresonant). We will need to determine whether they lie above or below the real axis.

The simplest pole to analyse is the critical one at $q = q_c$. From (5.1) it is clear that this pole can lie inside the contour only if $q_c > 0$, i.e. $\cos\theta < 0$, and in this case it will be shifted above the complex axis, and hence contribute to the far field only if $\cos(\theta - \phi) > 0$.

The propagating pole is a little more involved. For the pole to lie within the integration path it is necessary that a solution $q_0 > 0$ of (4.15) exists, and that the pole is shifted to the appropriate side of the axis, either above or below depending on how the contour is closed. With

$$\Gamma'(q_0) = 1 + \frac{F^2 h}{\sinh^2 q_0 h} \tag{5.3}$$

it is quite obvious that $\Gamma'(q_0) > 0$ for all positive q_0, so the position of the pole (5.2) is decided by the sign of $\Phi(q_0)$. However, by using (4.15) we may write

$$\Phi(q_0) = F^2 \coth(q_0 h) + q_0, \tag{5.4}$$

which again is clearly a positive quantity provided that $q_0 > 0$. Hence, both poles lie above the complex axis provided that $q_0, q_c > 0$ and contribute to the far field provided that $\cos(\theta - \phi) > 0$.

As discussed in § 4, a solution $q_0(\theta)$ exists for all θ and all values of F^2 and σ so long as h is finite, but $q_0(\theta)$ tends to zero in a sector $|\theta| > \theta_0$ when $h \to \infty$. Within this sector no far-field propagating wave exists in this limit.

5.1. *Resonance*

The 2D case considered in E&T uncovered that a resonance may occur between the regular downstream propagating wave and the critical wave (which only occurs downstream) if their wavenumbers are the same. In the present 3D configuration, we henceforth distinguish between a subresonant and a super-resonant regime. Physically, resonance occurs when the regular wave propagating in direction $\theta = \pi$ has the same phase velocity as the critical wave, i.e. the same velocity as the fluid current at depth $z = -D$. We note how this differs fundamentally from the Doppler resonance that may occur for a source that moves relative to the surface: in that case it is the group velocity that causes resonance when it coincides with the current velocity (e.g. Wehausen & Laitone 1960).

The situation that we define as subresonant occurs for parameters F^2 and σ that are such that $q_0(\theta) \neq q_c(\theta)$ for all θ. In this case the two poles in the integrand of (4.11) can be treated independently. In other words, in the subresonant regime the downstream regular wave and the critical layer wave have very different appearance and behaviour, and their individual contributions to the far field are easily identifiable. At a deeper level, this is because the critical layer wave can never satisfy the dispersion relation $\Gamma(\boldsymbol{q}) = 0$ when F^2 is subresonant.

The criterion for the situation to be subresonant is that $\Gamma(q_c, \theta) \neq 0$ for all θ. The equation $\Gamma(q_c, \theta) = 0$ may be written as

$$F^2 = \frac{1}{\sigma \cos\theta \left(\coth \dfrac{h}{\sigma \cos\theta} - \sigma \cos\theta \right)}. \tag{5.5}$$

In subcritical situations, this equation has no solution for any θ. The right-hand side is either always greater than F^2 or, in some cases when $\sigma, h > 1$, can be negative for some θ. Since F^2 is positive by definition, its resonant value is the smallest value for which (5.5) has a solution, corresponding to the smallest positive value of the right-hand side of (5.5). These positive minima occur at $\theta = 0, \pm\pi$ when $\sigma < 0.5$, but above some h-dependent value of σ the minima are found instead at two values of θ either side of 0 and π. After this bifurcation, the minimum value of F_{res} remains constant for higher values of σ. We define

$$F_{res}^2 = \min_{\theta, >0} \left\{ \frac{1}{\sigma \cos\theta \left(\coth \dfrac{h}{\sigma \cos\theta} - \sigma \cos\theta \right)} \right\}. \tag{5.6}$$

The notation means that the minimum value is found with respect to θ, but so that that negative values are ignored.

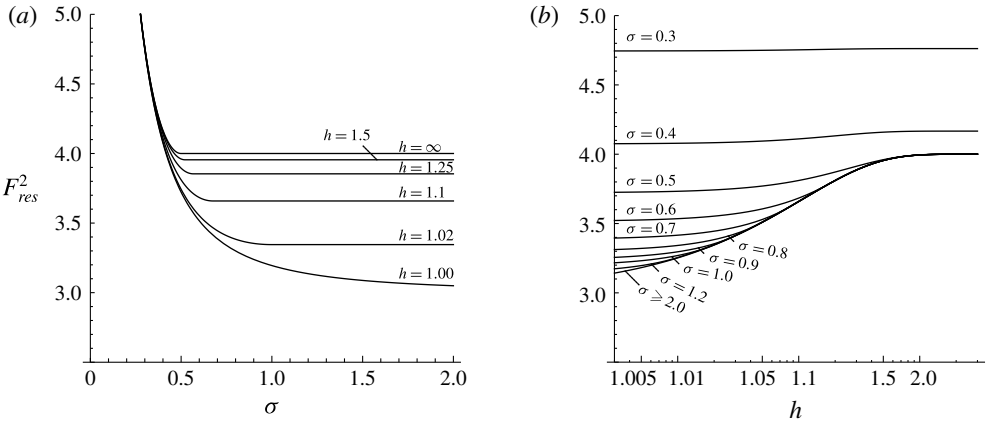

FIGURE 4. Plots of F^2_{res} as a function of σ for different values of h (a) and as a function of h for different σ (b). Any $h \gtrsim 2$ has F_{res} virtually indistinguishable from infinite depth.

One may show that if $\coth(h/\sigma) < \sigma$, the right-hand side of (5.5) is negative in some sectors near $\theta = 0$ and π; no resonance is then possible in these sectors. A necessary but insufficient criterion is that both σ and h exceed 1. The phenomenon thus bears resemblance with deep-water cutoff, discussed in § 4.1.

We term the situation subresonant for values of F^2 smaller than F^2_{res}. In the super-resonant regime, $F^2 > F^2_{res}$, and there always exists a value of θ for which the critical wave satisfies the dispersion relation. At resonance, the critical wave satisfies the dispersion relation at one or two distinct values of θ corresponding to the minimum or minima in (5.6). The behaviour of F^2_{res} for different σ and h is shown in figure 4. For small σ, the critical wave satisfies the dispersion relation at $\theta = \pi$, and F^2 is a decreasing function of σ. For σ above some threshold value, however, the critical wave first satisfies the dispersion relation (i.e. the minimum of the function in (5.6)) for a pair of propagation angles either side of $\theta = \pi$. From this point on, F^2_{res} remains constant as σ is further increased.

The criterion for resonance is similar to that found in the 2D case, but the interpretation is now a little different. In two dimensions, resonance occurred only at the single value $F^2 = F^2_{res}$. At this value, waves continued to grow indefinitely in amplitude away from the source as a linear function of difference, while at values above or below F^2_{res} the wave amplitude remained bounded everywhere. A study of the behaviour of F^2_{res} as a function of h and σ was given in E&T and need not be repeated here. Here, the situation is different mathematically in that a confluence of the two poles will occur at some θ for every value $F^2 > F^2_{res}$, although we shall see that also in the 3D case unbounded wave amplitudes can occur only exactly at the resonant value. Like in E&T, thus, the physical wave field only resonates at a single value $F^2 = F^2_{res}(\sigma, h)$.

5.2. *Subresonant case*

We assume now that $F^2 < F^2_{res}$, so that $q_0 \neq q_c$ for all θ. With reference to (4.11), let us define

$$G(\theta) = \int_0^\infty \mathrm{d}q f(q, \theta) \tag{5.7}$$

and note that

$$\mathrm{Res}_{q=q_0} f(q,\theta) = \frac{\mathrm{e}^{\mathrm{i}q_0\tilde{r}\cos(\theta-\phi)}}{\Gamma'(q_0)\sinh q_0 h}\left[\cosh q_0(h-1) + \frac{\sinh q_0(h-1)}{q_0 - q_c}\right], \tag{5.8a}$$

$$\mathrm{Res}_{q=q_c} f(q,\theta) = \frac{\mathrm{e}^{\mathrm{i}q_c\tilde{r}\cos(\theta-\phi)}}{\Gamma(q_c)}\frac{\sinh q_c(h-1)}{\sinh q_c h}. \tag{5.8b}$$

We bear in mind that the polar angle θ is the angle in the $\boldsymbol{q}$ Fourier plane and ϕ is the angle in the $\tilde{x},\tilde{y}$ plane. The integral around the closed contour Λ gets no contribution from the circular arc at infinity and is now

$$\begin{aligned}\oint_\Lambda \mathrm{d}q f(q,\theta) &= F(\theta) + F_{conn.}(\theta)\\ &= 2\pi\mathrm{i}[\mathrm{Res}_{q=q_0} f(q,\theta) + \Theta(-\cos\theta)\mathrm{Res}_{q=q_c} f(q,\theta)]\Theta[\cos(\theta-\phi)].\end{aligned} \tag{5.9}$$

Here, $F_{conn.}(\theta)$ is the integral along the connection path, as shown in figure 3, directed towards the origin.

We ascertain numerically that the contribution from the connection path falls off faster than the far field as $\tilde{r}\to\infty$ (it is possible, but cumbersome, to show this analytically using asymptotic methods). Hence, we shall identify the contribution from the poles as the far field, while noting that the division of ζ into near field and far field is not a unique operation.

The far-field surface elevation in the subresonant case is thus

$$\begin{aligned}\tilde{\zeta}_{f.f.} &= \frac{\mathrm{e}^{-\mathrm{i}T}}{2\pi}\int_{\phi-\pi/2}^{\phi+\pi/2}\mathrm{d}\theta\,\frac{q_0\mathrm{e}^{\mathrm{i}q_0\tilde{r}\cos(\theta-\phi)}}{\Gamma'(q_0)\sinh q_0 h}\left[\cosh q_0(h-1)+\frac{\sinh q_0(h-1)}{q_0-q_c}\right]\\ &\quad+\frac{\mathrm{e}^{-\mathrm{i}T-\mathrm{i}\tilde{x}/\sigma}}{2\pi}\int_{\pi/2}^{3\pi/2}\mathrm{d}\theta\,\frac{q_c\mathrm{e}^{-\mathrm{i}(\tilde{y}/\sigma)\tan\theta}}{\Gamma(q_c)}\frac{\sinh q_c(h-1)}{\sinh q_c h}\Theta[\cos(\theta-\phi)],\end{aligned} \tag{5.10}$$

where we have inserted the definition of q_c in the exponent of the corresponding integral to highlight that the $\tilde{x}$ dependence is of a pure plane wave form.

In figure 5 we moreover show example numerical calculations of the full surface elevation from (4.16) as well as the asymptotic regular and critical waves and the numerical evaluation of the connection path integral which we identify as the near field. The graph shows with clarity that the sum of the three contributions exactly matches the full integral, as it should, a useful validation of the numerical code.

Let us study for a moment the last integral in (5.10), which gives the critical 'wave'. When $\tilde{r}$ grows large, the exponential function typically becomes rapidly oscillating, and the integral is a rapidly decreasing function of $\tilde{r}$ according to the Riemann–Lebesgue lemma (Bender & Orszag 1991, § 6.5). This is true everywhere in the $\tilde{r}$, ϕ plane except along the line $\phi=\pi$ (where $\tilde{y}=0$) where the exponent becomes independent of θ (this is also true at $\phi=0$, but this line is excluded from the integral by the Heaviside Θ function). What this implies is that the critical wave must die quickly away from the source in all directions except along the line $\phi=\pi$ where it takes the form

$$\tilde{\zeta}_{f.f.,c}(\tilde{x},\tilde{y}=0) = \frac{\mathrm{e}^{-\mathrm{i}T-\mathrm{i}\tilde{x}/\sigma}}{2\pi}\Theta(-\tilde{x})\int_{\pi/2}^{3\pi/2}\mathrm{d}\theta\,\frac{q_c}{\Gamma(q_c)}\frac{\sinh q_c(h-1)}{\sinh q_c h}. \tag{5.11}$$

The integral is now just a constant with respect to x, and the behaviour along the ray $\phi=\pi$ is a wave of dimensionless wavelength $\lambda_c = 2\pi\sigma$, as found for the critical layer

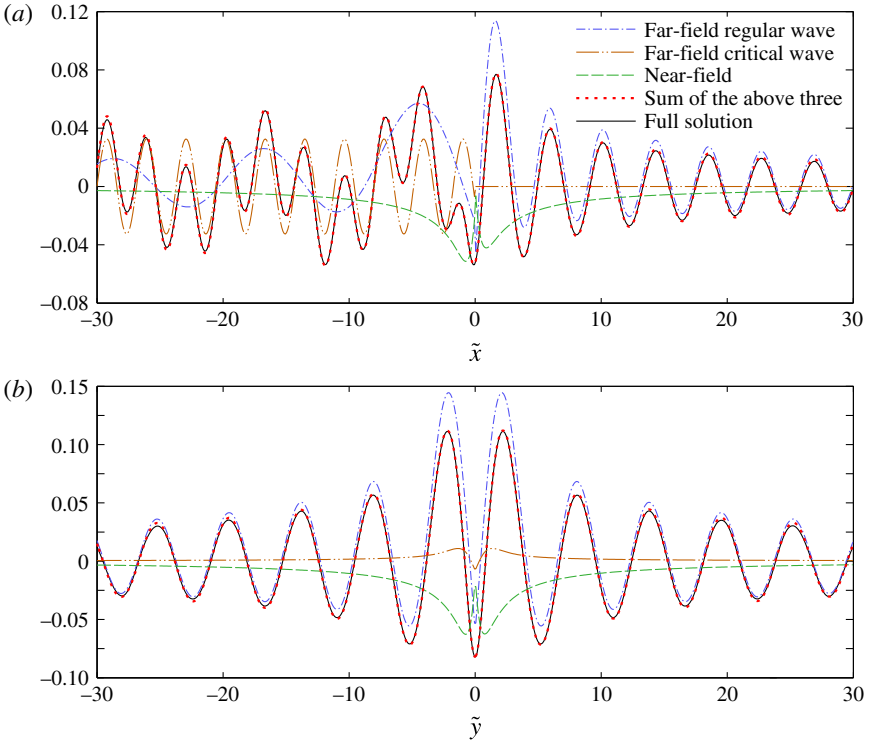

FIGURE 5. (Colour online) Plots along the $\tilde{x}$ axis at $\tilde{y}=0$ (a) and along the $\tilde{y}$ axis at $\tilde{x}=0$ (b) of the full surface elevation calculated from (4.16) (solid line) as well as numerical calculation of the far fields from regular as well as critical waves, and numerical calculation of the near field from the connection integration path shown in figure 3. The parameters in this example are $F^2=1$, $\sigma=0.5$, $h=4$, $T=0.3$.

wave also in the 2D case by E&T; $\lambda_c D$ is the distance travelled during one oscillation period by a fluid particle at depth $z=-D$.

The deep-water limit of $\tilde{\zeta}_{f.f.}$ is

$$\tilde{\zeta}_{f.f.} \xrightarrow{h\to\infty} \frac{\mathrm{e}^{-\mathrm{i}T}}{2\pi}\int_{-\theta_0}^{\theta_0} \mathrm{d}\theta\, q_0 \mathrm{e}^{\mathrm{i}q_0\tilde{r}\cos(\theta-\phi)-q_0}\left(1+\frac{1}{q_0-q_c}\right)\Theta[\cos(\theta-\phi)] + \frac{\mathrm{e}^{-\mathrm{i}T-\mathrm{i}\tilde{x}/\sigma}}{2\pi}\int_{\pi/2}^{3\pi/2}\mathrm{d}\theta\,\frac{q_c \mathrm{e}^{\mathrm{i}(\tilde{y}/\sigma)\tan\theta-q_c}}{q_c-F^2(1+\sigma\cos\theta)}\Theta[\cos(\theta-\phi)], \tag{5.12}$$

with θ_0 defined in (4.6).

Numerical examples of subresonant wave fields are shown in figure 6 for increasing values of σ. The asymptotic far-field expressions are reasonable approximations for distances more than a couple of wavelengths from the source, and are numerically far quicker and also easier to calculate. Numerical evaluation of the full expression in (4.16) is considerably more subtle than the corresponding calculation in the 2D case, because it is necessary to use a smaller value of ϵ when going to $\tilde{r}$ as large as 30, giving very sharp contributions near the poles, making brute force methods based on adaptive grid refinement very slow to converge. The chosen method was to calculate

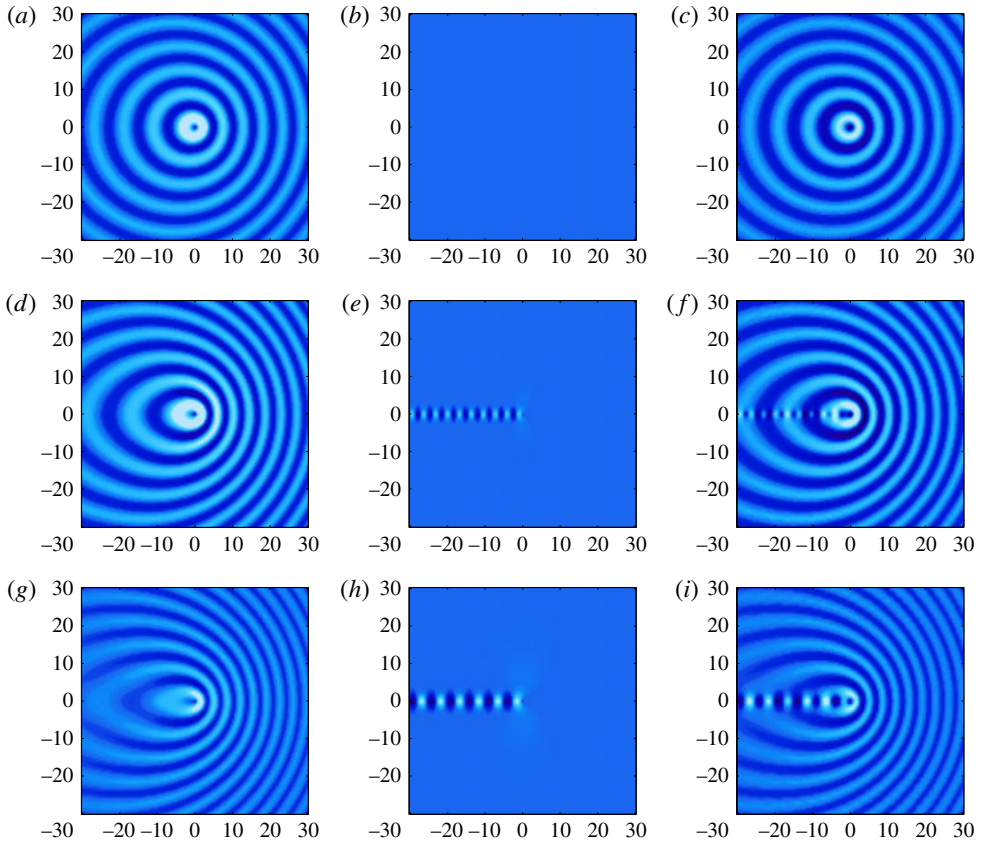

FIGURE 6. (Colour online) Relief plots of the typical subresonant wave field in the $\tilde{x}, \tilde{y}$ plane from an oscillating source with $F^2 = 1$, $h = 4$ and $\sigma = 0.2$, 0.5 and 0.8 (*a–c*, *d–f*, *g–i*) at time $T = 0.3$. (*a*,*d*,*g*) Far-field solution for only the regular wave. (*b*,*e*,*h*) Far-field solution for only the critical wave. (*c*,*f*,*i*) Full solution calculated from (4.16) with $\epsilon = 0.001$. The colour scaling is the same within each row. For (*a–c*), the amplitude of the critical wave is so small as to be invisible.

the positions of the poles before integrating, then precalculate an integration grid with much finer resolution near poles, whereupon integration was performed without further grid refinement. This method was able to speed up the integration by two orders of magnitude, at the expense of not knowing the exact integration accuracy, which was no problem in our case since both the far-field and near-field solutions could be calculated arbitrarily accurately, providing a benchmark and convergence check such as that shown in figure 5.

5.3. *Deep or shallow water?*

The terms ‘deep’ or ‘shallow’ water in relation to surface waves are determined by the ratio of wavelength to water depth. While our dimensionless units were found to produce the best set of parameters (F^2, h, σ) to characterise the wave field in different situations, they somewhat disguise the effect of water depth since h is a measure of how close the source is to the surface or bottom, and bears no relation to the wavelength.

Our subresonant far-field considerations reveal, however, that no single parameter on its own can hope to determine whether the system is 'shallow' or 'deep', simply because the critical waves and regular waves can have very different wavelengths. The criterion for a wave $\boldsymbol{q}$ to be of 'deep water' kind is that $qh \gg 1$. Now, as we have seen, regular waves in deep water have wavenumbers of approximately $F^2(1+\sigma\cos\theta)$ (but see the discussion of 'cutoff' above, for the case when $1+\sigma\cos\theta<0$), hence the criterion for regular waves to be 'deep', at least in some directions, is that $F^2(1+\sigma)h \gg 1$. On the other hand, the dimensionless wavenumber of the critical wave is $1/\sigma$ directly downstream, so the criterion that the critical wave is 'deep water' is that $h \gg \sigma$. Often, the critical wave will be 'deep water' in the subresonant regime even though the regular wave might be affected by the presence of finite depth.

5.4. *Asymptotic critical wave*

A case that is particularly suited for asymptotic analysis is when the shear is relatively weak or the frequency is high, so that we may assume $\sigma \ll 1$. With this assumption, the factor $\exp(-1/\sigma\cos\theta)$ in the integrand of the critical wave term of (5.10) means that only angles θ close to $\theta=\pi$ will contribute since the exponential is otherwise very small. We let $\beta=\theta-\pi$ and approximate the integral using Laplace's method (Bender & Orszag 1991, §6.4) by expanding the exponent around $\beta=0$ and taking $\beta=0$ elsewhere. Using

$$q_c\cos(\theta-\phi)\sim-\frac{1}{\sigma}(\cos\phi+\beta\sin\phi+O(\beta^3)),\quad q_c\sim\frac{1}{\sigma}\left(1+\frac{1}{2}\beta^2+O(\beta^4)\right), \tag{5.13a,b}$$

the critical layer term is approximately

$$\begin{aligned}\tilde{\zeta}_{f.,c}(\tilde{x},\tilde{y}) &\sim \frac{(1/\sigma)\mathrm{e}^{-\mathrm{i}T-\mathrm{i}\tilde{x}/\sigma}}{2\pi\Gamma(1/\sigma,\pi)}\frac{\sinh\dfrac{h-1}{\sigma}}{\sinh\dfrac{h}{\sigma}}\Theta(-\tilde{x})\int_{-\infty}^{\infty}\mathrm{d}\beta\,\mathrm{e}^{-\mathrm{i}(\tilde{y}/\sigma)\beta-\beta^2/2\sigma}\\ &\sim \frac{\sinh\dfrac{h-1}{\sigma}}{\Gamma(1/\sigma,\pi)\sinh\dfrac{h}{\sigma}}\Theta(-\tilde{x})\mathrm{e}^{-\mathrm{i}T-\mathrm{i}\tilde{x}/\sigma}\frac{1}{\sqrt{2\pi\sigma}}\mathrm{e}^{-\tilde{y}^2/2\sigma}\end{aligned} \tag{5.14}$$

when $\sigma \ll 1$, where

$$\Gamma(1/\sigma,\pi)=\frac{1}{\sigma}-F^2\left(\coth\frac{h}{\sigma}-\sigma\right). \tag{5.15}$$

We see that the surface elevation from the critical layer is restricted to a thin area close to the $\tilde{x}$ axis downstream of the wave of constant thickness $\sim\sqrt{\sigma}$, falling off away from the axis in a Gaussian manner. In the absence of dissipation, it does not decay away from the source, as is required by energy conservation in linear theory, since the critical wave does not spread but travels downstream atop a row of vortices.

Although we assumed σ small, (5.14) is in fact a fair representation of the critical wave in subresonant cases for $\sigma \lesssim 0.4$. In any case, the critical wave always has the simple form $\tilde{\zeta}_{f.,c}\sim f(\tilde{y})\exp(-\mathrm{i}T-\mathrm{i}\tilde{x}/\sigma)$, where the function $f(\tilde{y})$ is an integral that is simple to evaluate numerically,

$$f(\tilde{y})=\frac{1}{2\pi}\int_{\pi/2}^{3\pi/2}\mathrm{d}\theta\,\frac{q_c\cos[(\tilde{y}/\sigma)\tan\theta]}{\Gamma(q_c,\theta)}\frac{\sinh q_c(h-1)}{\sinh q_c h}, \tag{5.16}$$

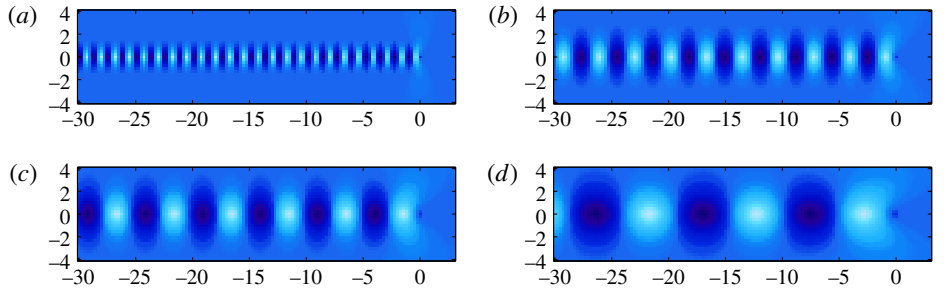

FIGURE 7. (Colour online) Relief plots of a subresonant critical wave in the $\tilde{x}, \tilde{y}$ plane for increasing values of σ: $\sigma = 0.2$ (*a*), 0.5 (*b*), 0.8 (*c*), 1.5 (*d*). In all graphs, $F^2 = 1$, $h = 4$. The colours are scaled individually in each panel and do not reflect relative amplitudes, which depend strongly on σ.

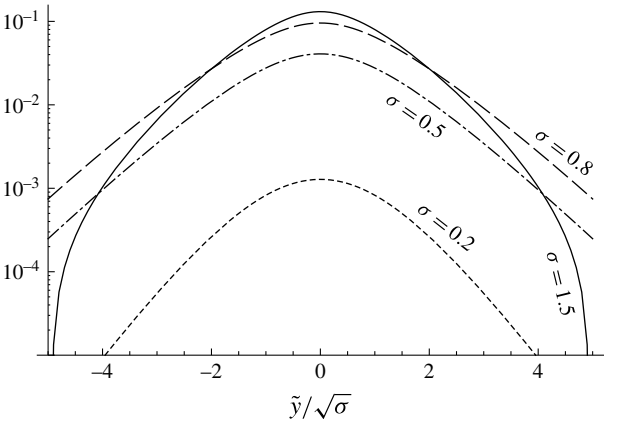

FIGURE 8. The asymptotic amplitude function $f(\tilde{y})$ for the critical waves shown in figure 7.

when $|\tilde{x}| \gg \tilde{y}$ (i.e. $\phi \approx \pi$). The amplitude function $f(\tilde{y})$ for the four cases shown in figure 7 is shown in figure 8. The distribution has an approximately Gaussian shape with half-width $\sim\sqrt{\sigma}$ when $\sigma \lesssim 1$, but becomes distinctly non-Gaussian when $\sigma > 1$.

The phase velocity of the critical wave in dimensional units is easily found to be *SD*, meaning that the critical 'wave' is in fact the surface manifestation of an underwater row of flow structures which are convected with the mean flow, in the same way as found in the 2D case. Also similar to the 2D case, the amplitude of the critical wave diverges when $\Gamma(1/\sigma, \pi) \to 0$, in accordance with the resonance criterion of (5.6).

5.5. *Asymptotic regular wave*

The regular wave far-field expression, the first term of (5.10), may be approximated further for large $\tilde{r}$ by use of the stationary phase approximation. At large $\tilde{r}$, the integrand generally oscillates rapidly as $\exp(\mathrm{i}\tilde{r}\varphi(\theta))$, where the exponent function is

$$\varphi(\theta) = q_0(\theta)\cos(\theta - \phi). \tag{5.17}$$

At large distances, the integral will be dominated by the value of θ where $\varphi'(\theta)=0$, i.e. a stationary point. Let the stationary point be called θ_s. It is not possible to find explicit solutions for θ_s, but it may be defined implicitly and solved numerically.

Using the stationary phase approximation (Bender & Orszag 1991), the regular far-field integral becomes, to leading order in $1/\tilde{r}$,

$$\tilde{\zeta}_{f.f.,r}(\tilde{r},\phi)\sim\frac{q_{0s}\mathrm{e}^{\mathrm{i}\tilde{r}\varphi(\theta_s)-\mathrm{i}T+\mathrm{sign}[\varphi''(\theta_s)]\pi/4}}{\Gamma'(q_{0s})\sinh q_{0s}h\sqrt{2\pi\tilde{r}|\varphi''(\theta_s)|}}\left[\cosh q_{0s}(h-1)+\frac{\sinh q_{0s}(h-1)}{q_{0s}-q_c(\theta_s)}\right], \tag{5.18}$$

where we use the shorthand $q_{0s}=q_0(\theta_s)$ (note that $\Gamma(q,\theta)$ is a function of both q and θ while $\Gamma'(q)$ is a function of q only).

It is worth noting before proceeding how the critical wave affects the amplitude of the regular wave indirectly, through the last term in the brackets in (5.18). In the 2D case (E&T), the corresponding term was responsible for the regular wave being different in amplitude from that predicted by potential theory, sometimes radically so. In three dimensions, no potential theory exists of course, but at least in the subresonant regime it is still meaningful to consider this term as the amplitude correction to the regular wave stemming from the fact that part of the mass flux from the source must go into the critical wave.

To calculate this asymptotic wave, we must find θ_s and q_{0s} by solving a combined system of equations: the dispersion relation (4.15) and $\varphi'(\theta_s)=0$, which read respectively

$$\Gamma(q_{0s},\theta_s)=0\quad\text{and}\quad q_0'(\theta_s)\cos(\theta_s-\phi)-q_0(\theta_s)\sin(\theta_s-\phi)=0. \tag{5.19}$$

We require the following relations, obtained by noting that q_0 satisfies $\Gamma(q_0,\theta)=0$:

$$\Gamma'(q_0) = 1+hF^2[\coth^2 q_0h-1], \tag{5.20a}$$
$$\Gamma''(q_0) = -2h^2F^2\coth q_0h[\coth^2 q_0h-1], \tag{5.20b}$$
$$\coth q_0h = q_0/F^2-\sigma\cos\theta, \tag{5.20c}$$
$$\varphi''(\theta) = q_0''(\theta)\cos(\theta-\phi)-2q_0'(\theta)\sin(\theta-\phi)-q_0(\theta)\cos(\theta-\phi), \tag{5.20d}$$
$$q_0'(\theta) = -\sigma F^2\sin\theta/\Gamma'(q_0), \tag{5.20e}$$
$$q_0''(\theta) = -\sigma F^2\cos\theta/\Gamma'(q_0)-(\sigma F^2\sin\theta)^2\Gamma''(q_0)/[\Gamma'(q_0)]^3. \tag{5.20f}$$

In deep water, the calculation is significantly simpler; the asymptotic regular wave now reads

$$\tilde{\zeta}_{f.f.,r}(\tilde{r},\phi)\sim\frac{q_{0s}\mathrm{e}^{\mathrm{i}\tilde{r}\varphi(\theta_s)-\mathrm{i}T+\mathrm{sign}[\varphi''(\theta_s)]\pi/4}}{\sqrt{2\pi\tilde{r}|\varphi''(q_{0s})|}}\mathrm{e}^{-q_{0s}}\left[1+\frac{1}{q_{0s}-q_c(\theta_s)}\right], \tag{5.21}$$

with $q_{0s}=F^2(1+\sigma\cos\theta_s)$, and where θ_s solves

$$\sigma\sin(2\theta_s-\phi)+\sin(\theta_s-\phi)=0. \tag{5.22}$$

In fact, an explicit solution to this equation exists, but it is sufficiently complicated that numerical evaluation was found to be preferable. Moreover, the evaluation of $\varphi''(q_0)$ is now simple, with $q_0'(\theta)=-\sigma F^2\sin\theta$ and $q_0''(\theta)=-\sigma F^2\cos\theta$.

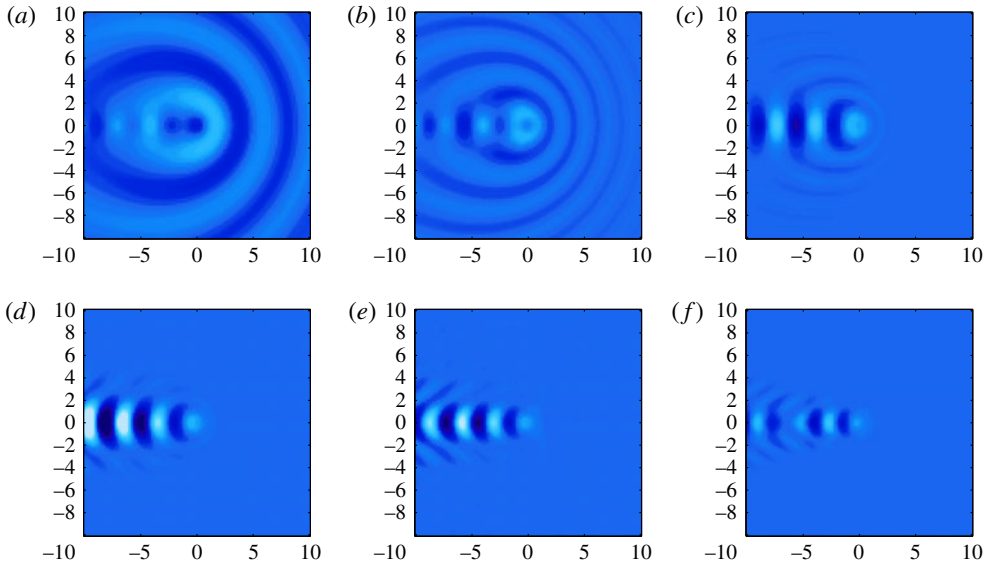

FIGURE 9. (Colour online) Relief plots of the wave field $\tilde{\zeta}(\tilde{x}, \tilde{y})$ for increasing values of F^2 from subresonant to super-resonant: $F^2 = 1$ (*a*), 2 (*b*), 3 (*c*), 4 (*d*), 5 (*e*), 6 (*f*). In all graphs, $\sigma = 0.5$, $h = 4$, $\epsilon = 0.01$ and $T = 0.3$. The colour range is from -0.2 (black) to 0.2 (white).

5.6. *Resonant case*

The qualitative behaviour of the waves as F^2 is brought from subresonant to super-resonant may be seen from figure 9, here for a moderate value of the shear, $\sigma = 0.5$, and essentially deep water, $h = 4$. The value of F^2_{res} is 3.9999982, so the case $F^2 = 4.0$ illustrates the resonating frequency. At low values of F^2, the regular propagating waves dominate, with the critical wave only a minor correction. As F^2 increases, the regular wave rapidly disappears, as may understood by regarding the asymptotic deep-water far-field expression, (5.21), where we see the amplitude of the regular waves decreasing as $\exp(-q_0)$. Since $q_0 \propto F^2$ in deep water, it is clear that the critical wave must dominate as F^2 grows larger, because q_c is independent of F^2 and no corresponding exponential decrease is found for the critical wave. Near $\phi = \pi$, however, the regular waves do not vanish, because regular waves of wavelength close to the wavelength of the critical wave are amplified. Within a wedge around $\phi = \pi$, also the regular waves continue to grow when resonance is approached, interfering strongly with the critical wave. At $\phi = \pi$, thus, the behaviour is similar to that obtained in two dimensions; the regular and critical waves each diverge in amplitude as $F^2 \to F^2_{res}$, but the combined wave increases linearly in amplitude as a function of $|x|$ downstream. This is shown in figure 10.

The wave pattern at (or close to) resonance is mainly found downstream. Its appearance is that of the critical wave, with regular wave 'fringes'. The combined wave near resonance moreover increases linearly in width downstream, covering a constant angle. At the centre of the wedge, the typical critical wave pattern is found, with regular waves outside it producing a herringbone pattern. The waves are contained within a wedge angle that depends on σ.

When the Froude number increases beyond F^2_{res}, wave amplitudes no longer grow indefinitely in the downstream direction, but are modulated in the manner typical of

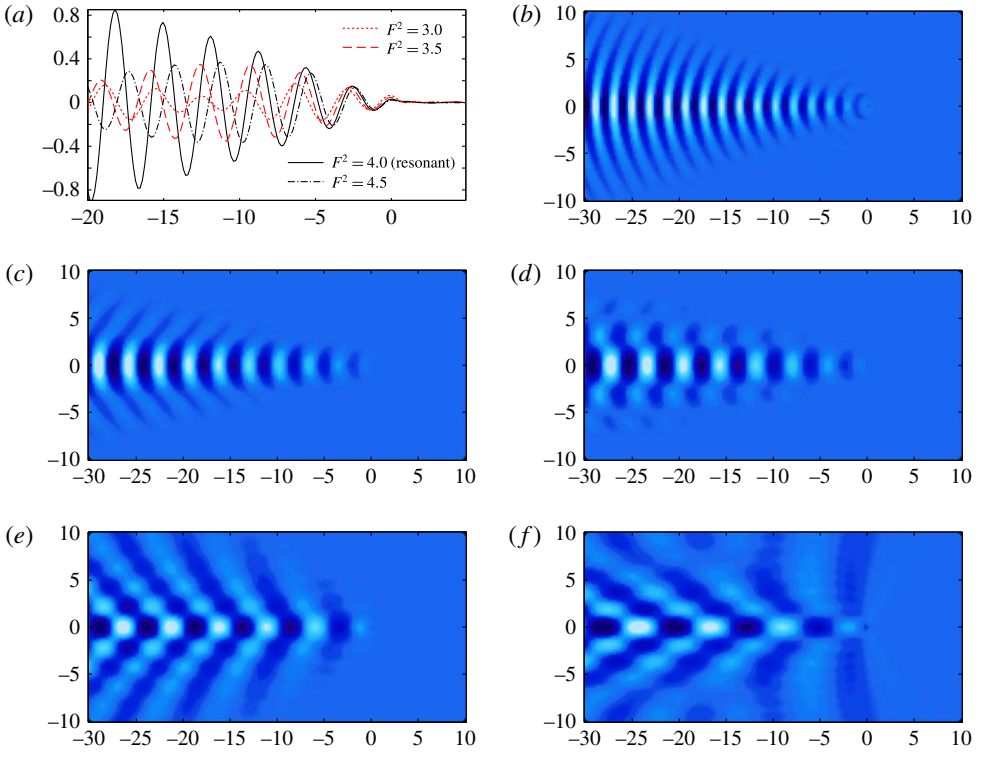

FIGURE 10. (Colour online) (*a*) Plots of $\tilde{\zeta}(\tilde{x}, \tilde{y}=0)$ showing the transition from sub- to super-resonant for $\sigma = 0.5$, $h = 4$. (*b–f*) Relief plots which show $\tilde{\zeta}_{f.f.}(\tilde{x}, \tilde{y})$ for F^2 close to the resonant value (we choose $F^2 = F^2_{res} - 0.1$) to illustrate the behaviour at resonance: $\sigma = 0.3$ (*b*), 0.5 (*c*), 0.6 (*d*), 0.8 (*e*), 1.2 (*f*). According to (5.6) with $h = 4$, the Froude number is $F^2 = 4.66$ for $\sigma = 0.3$, and $F^2 = 3.9$ for the remaining relief plots. We have $T = 0.3$ everywhere.

interfering waves with similar but unequal wavelength. The pattern remains within a downstream wedge, and distinct contributions from regular and critical waves once again become visible, although the formal splitting into a two-component far field is no longer possible in the manner of § 5.2.

6. Some notes on the velocity field

We provide here the formulae for the velocity field, although a detailed analysis of the velocity field as a function of coordinates as well as parameters σ, F^2 and h is a major undertaking which we largely leave for a later investigation.

We found the vertical velocity component in § 3 as

$$w(\tilde{z}) = A \sinh q(\tilde{z}+h) + \left[\cosh q(\tilde{z}+1) - \frac{\sinh q(\tilde{z}+1)}{q - q_c}\right] \Theta(\tilde{z}+1), \tag{6.1}$$

with

$$A(\boldsymbol{q}) = \frac{1}{\Gamma(\boldsymbol{q})}\left[\left(F^2 + \frac{q - \sigma F^2 \cos\theta}{q - q_c}\right)\frac{\sinh q}{\sinh qh} - \left(q - \sigma F^2 \cos\theta + \frac{F^2}{q - q_c}\right)\frac{\cosh q}{\sinh qh}\right], \tag{6.2}$$

where $\Gamma(\boldsymbol{q}) = q - F^2(\coth qh + \sigma\cos\theta)$ as before. We note the correspondence with Section 6 of E&T. Elimination of the pressure from (2.11*b*) and (2.11*c*) gives

$$v'(\tilde{z}) - \frac{\sigma q_x}{1-\sigma q_x\tilde{z}}v(\tilde{z}) = \mathrm{i}q_y w(\tilde{z}). \tag{6.3}$$

The homogeneous solution of this equation,

$$v_{homog.} = \frac{C}{1-\sigma q_x\tilde{z}}, \tag{6.4}$$

can only agree with the dynamic boundary condition (2.5*b*) if $C=0$. The solution is thus the particular solution only, given by

$$\begin{aligned} v(\tilde{z}) \;=\; & \frac{\mathrm{i}q_y}{q}\left(A(\boldsymbol{q})\cosh q(\tilde{z}+h) + \frac{\sigma q_x}{q(1-\sigma q_x\tilde{z})}A(\boldsymbol{q})\sinh q(\tilde{z}+h)\right. \\ & + \left\{\left[1 - \frac{\sigma q_x}{q(q-q_c)(1-\sigma q_x\tilde{z})}\right]\sinh q(\tilde{z}+1)\right. \\ & \left.\left. - \left[\frac{1}{q-q_c} - \frac{\sigma q_x}{q(1-\sigma q_x\tilde{z})}\right]\cosh q(\tilde{z}+1)\right\}\Theta(\tilde{z}+1)\right). \end{aligned} \tag{6.5}$$

Use of the continuity equation (2.9) then gives

$$\begin{aligned} u(\tilde{z}) \;=\; & \frac{\mathrm{i}q_x}{q}\left(A(\boldsymbol{q})\cosh q(\tilde{z}+h) - \frac{\sigma q_y^2}{qq_x(1-\sigma q_x\tilde{z})}A(\boldsymbol{q})\sinh q(\tilde{z}+h)\right. \\ & + \left\{\left[1 + \frac{\sigma q_y^2}{qq_x(q-q_c)(1-\sigma q_x\tilde{z})}\right]\sinh q(\tilde{z}+1)\right. \\ & \left.\left. - \left[\frac{1}{q-q_c} + \frac{\sigma q_y^2}{qq_x(1-\sigma q_x\tilde{z})}\right]\cosh q(\tilde{z}+1)\right\}\Theta(\tilde{z}+1)\right). \end{aligned} \tag{6.6}$$

A noteworthy difference from the 2D case (E&T) is that the expressions for u and v have two distinct poles, each corresponding to critical layer-type solutions. Inspection of (6.5) and (6.6) reveals that, in addition to the poles for the regular wave where $\Gamma(\boldsymbol{q})=0$, there are critical layer-type poles both at $q=q_c(\theta)$ and at $q=1/(\sigma\cos\theta\tilde{z}) = q_c/|\tilde{z}|$.

The wavenumber q_c was discussed above, and at length in the 2D case in E&T. It is the wavenumber associated with the string of vortical flow structures generated as the source injects additional vorticity into the flow as discussed in § 2.1. These vortices have spatial periodicity ('wavelength') $2\pi/q_c$ in dimensionless units.

On the other hand, $q=q_c/|\tilde{z}|$, or in dimensional terms $\omega/k\cos\theta = U(z)$, describes a 'wave' moving downstream instead at the same velocity as the flow at depth $\tilde{z}$, and is caused instead by flow structures at that level. Like the critical wave, this 'wave' (visible only in horizontal velocity components) is also only present downstream of the source. Thus, unlike the vertical velocity w, the horizontal velocity components are affected in the far field by drifting flow structures from the source not only at the single depth $\tilde{z}=-1$ but at all depths. A careful study of the resulting velocity field as well as the vorticity transport from the source into the critical layer is likely to reveal interesting and novel insights, but is a major undertaking beyond the scope of the present paper.

7. Summary and conclusions

The oscillating point source in a shear flow of uniform vorticity S with a free surface is analysed analytically in the framework of the Euler equation, linearised with respect to perturbation quantities. The analysis is thus a natural extension of the corresponding effort in two dimensions by Ellingsen & Tyvand (2016) (shorthand E&T). The submergence depth of the source is D, the constant water depth is H and the oscillation frequency is ω. The terms 'upstream' and 'downstream' are as seen from a system where the source and undisturbed surface are at rest.

The wave field due to the oscillating source is characterised by contributions from two distinct types of waves: the regular propagating dispersive waves which satisfy the dispersion relation in the presence of a shear current and a set of waves resulting from the formation of a critical layer-like subsurface flow below the surface which is advected downstream of the source. The latter 'critical wave' typically has the form of a narrow train of waves of constant width and wavelength which remains unchanged in shape and amplitude as it is swept downstream with the background flow. In the 2D case, it was straightforward to show that the critical layer corresponded to vortical flow structures akin to Kelvin's cat's eye vortices, centred at the depth of the source. A full analysis of the velocity field in the 3D case is more involved and will be considered in a future paper. However, inspection of the vorticity equation reveals that exactly the same mechanism is at play in the 3D flow as was analysed at length in E&T. The resulting thin line of undulating vorticity directly downstream of the source is quite distinct from the vorticity perturbations always present in 3D shear flow whenever waves propagate at oblique angles with the shear flow, and shift and twist the background vortex lines they pass (Ellingsen 2016). In the present system, both vorticity perturbations are present.

In similar manner to the 2D case considered in E&T, a cutoff of regular waves in some downstream directions occurs in the limit of deep water when the shear S exceeds ω. In two dimensions the result was that the downstream regular wave disappears, whereas in the 3D case all regular waves vanish for propagation directions inside a 'forbidden' sector of propagation angles in downstream directions. When $S/\omega \to \infty$, the width of the forbidden sector approaches π, covering all directions with a downstream component. When the water depth is finite, regular waves may propagate in all directions, and for large but finite depth, the 'forbidden' sector is instead characterised by regular waves of long wavelengths and small amplitudes.

We define three non-dimensional parameters to characterise the flow: the relative depth $h = H/D$, the dimensionless shear $\sigma = S/\omega$ and the (squared) Froude number $F^2 = \omega^2 D/g$. At a particular resonant value $F^2_{res}(\sigma, h)$ of the Froude number, the downstream regular and critical waves resonate. A clear distinction between regular waves and critical waves can only be made at subresonant Froude numbers, and we provide asymptotic expressions for the far-field wave patterns in the subresonant case. As F^2 approaches the resonant value, resonance results in a wave field that grows linearly with distance from the source and that is contained within a downstream wedge symmetrical about $y = 0$.

Supplementary Movies

Supplementary Movies is available at http://dx.doi.org/10.1017/jfm.2016.293.

REFERENCES

BENDER, C. M. & ORSZAG, S. A. 1991 *Advanced Mathematical Methods for Scientists and Engineers*. Springer.

BOOKER, J. R. & BRETHERTON, F. P. 1967 The critical layer for internal gravity waves in a shear flow. *J. Fluid Mech.* **27**, 513–539.

CONSTANTIN, A. 2011 Two-dimensionality of gravity water flows of constant nonzero vorticity beneath a surface wave train. *Eur. J. Mech. (*B*/Fluids)* **30**, 12–16.

CONSTANTIN, A. & VARVARUCA, E. 2011 Steady periodic water waves with constant vorticity: regularity and local bifurcation. *Arch. Rat. Mech. Anal.* **199**, 33–67.

DYER, K. R. 1971 Current velocity profiles in a tidal channel. *Geophys. J. Intl* **22**, 153–161.

EHRNSTRÖM, M. & VILLARI, G. 2008 Linear water waves with vorticity: rotational features and particle paths. *J. Differ. Equ.* **244**, 1888–1909.

ELLINGSEN, S. Å. 2014*a* Initial surface disturbance on a shear current: the Cauchy–Poisson problem with a twist. *Phys. Fluids* **26**, 082104.

ELLINGSEN, S. Å. 2014*b* Ship waves in the presence of uniform vorticity. *J. Fluid Mech.* **742**, R2.

ELLINGSEN, S. Å. 2016 Oblique waves on a vertically sheared current are rotational. *Eur. J. Mech. (*B*/Fluids)* **56**, 156–160.

ELLINGSEN, S. Å. & BREVIK, I. 2014 How linear surface waves are affected by a current with constant vorticity. *Eur. J. Phys.* **35**, 025005.

ELLINGSEN, S. Å. & TYVAND, P. A. 2016 Oscillating line source in a shear flow with a free surface: critical layer-like contributions. *J. Fluid Mech.* **798**, 201–231; (Preceding paper, referred to in the text as E&T).

FALTINSEN, O. M. 1990 *Sea Loads on Ships and Offshore Structures*. Cambridge University Press.

JOHNSON, R. S. 1990 Ring waves on the surface of shear flows: a linear and nonlinear theory. *J. Fluid Mech.* **215**, 145–160.

JONES, I. S. F. & TOBA, Y. (Eds) 2001 *Wind Stress Over the Ocean*. Cambridge University Press.

KOCHIN, N. E. 1939 The two-dimensional problem of steady oscillations of bodies under the free surface of a heavy incompressible fluid. *Izv. Akad. Nauk SSSR, Otdel. Tekhn. Nauk* **4**, 37–62.

KOCHIN, N. E. 1940 The theory of waves generated by oscillations of a body under the free surface of a heavy incompressible fluid. *Uchenye Zapiski Moskov Gos. Univ.* **46**, 86–106.

LI, Y. & ELLINGSEN, S. Å. 2015 Initial value problems for water waves in the presence of a shear current. In *Proceedings of the 25th International Offshore and Polar Engineering Conference (ISOPE)*, vol. 3, pp. 543–549. The International Society of Offshore and Polar Engineers (ISOPE).

LI, Y. & ELLINGSEN, S. Å. 2016 Ship waves on uniform shear current at finite depth: wave resistance and critical velocity. *J. Fluid Mech.* **791**, 539–567.

LIGHTHILL, J. 1978 *Waves in Fluids*. Cambridge University Press.

MELLOR, G. 2003 The three-dimensional current and surface wave equations. *J. Phys. Oceanogr.* **33**, 1978–1989.

NEWMAN, J. N. 1977 *Marine Hydrodynamics*. MIT Press.

PEREGRINE, D. H. 1976 Interaction of water waves and currents. *Adv. Appl. Mech.* **16**, 9–117.

SHEMDIN, O. H. 1972 Wind-generated current and phase speed of wind waves. *J. Phys. Oceanogr.* **2**, 411–419.

SHRIRA, V. I. 1993 Surface waves on shear currents: solution of the boundary-value problem. *J. Fluid Mech.* **252**, 565–584.

SOULSBY, R. L., HAMM, L., KLOPMAN, G., MYRHAUG, D., SIMONS, R. R. & THOMAS, G. P. 1993 Wave–current interaction within and outside the bottom boundary layer. *Coast. Engng* **21**, 41–69.

THOMSON, SIR W. 1880 On a disturbing infinity in Lord Rayleigh's solution for waves in a plan vortex stratum. *Nature* **23**, 45–46.

TYVAND, P, A. & LEPPERØD, M. E. 2014 Oscillatory line source for water waves in shear flow. *Wave Motion* **51**, 505–516.

TYVAND, P. A. & LEPPERØD, M. E. 2015 Doppler effects of an oscillating line source in shear flow with a free surface. *Wave Motion* **52**, 103–119.

WAHLÉN, E. 2009 Steady water waves with a critical layer. *J. Differ. Equ.* **246**, 2468–2483.

WEHAUSEN, J. W. & LAITONE, E. V. 1960 Surface waves. In *Fluid Dynamics III* (ed. S. Flügge), Encyclopedia of Physics, vol. IX, pp. 446–778. Springer.